AIAA AVIATION Forum
16-20 June 2014, Atlanta, GA
32nd AIAA Applied Aerodynamics Conference

10.2514/6.2014-3171

The Effects of Turbulence Model Corrections on Drag Prediction of NASA Common Research Model

Xiaoquan Gong[1]
Northwestern Polytechnical University, Xi'an, Shanxi, 710072, China

Jiangtao Chen[2], Naichun Zhou[3], Yaobing Zhang[4], Youqi Deng[5]
China Aeridynamics Research and Development Center, Mianyang, Sichuan, 621000, China

The effects of turbulence model corrections on drag prediction of NASA common research model are presented in this paper. The computations are accomplished with in-house flow solver MFlow, which is based on cell-center finite volume method and capable of handling arbitrary element type. The 2nd order accuracy in space is achieved with linear reconstruction in cells. Hexahedral grids and hybrid grids provided by the 5th Drag Prediction Workshop committee are taken into account. The original formulations of the turbulence model and rotation correction (RC) as well as quadratic constitutive relation (QCR) correction are considered to study the effects of different model corrections. Nearly linear grid convergence of drag coefficient with grid refinement is obtained for both hexahedral and hybrid grids under the lift condition of CL=0.5 with the original SA model. Drag coefficients predicted with fine and extra-fine hexahedral grid are within 2 cnts of experiment result obtained in National Transonic Facility. Pressure drag is more sensitive to grid refinement and grid type than viscous drag. The size of the separation bubble near the wing-body junction increases with grid refinement. All the aerodynamic curves with different model corrections show similar trends. Model corrections mainly influence the pressure prediction near the shock wave and main separation line. Relative to the original form, the model corrections, especially QCR, achieve larger pressure coefficient near shock wave which extends from wing tip to wing root. The location of shock wave is shifted upstream due to model corrections. Model corrections also influence the prediction of side-of-body bubbles. The size of the bubble is very close between results obtained with the original form and RC, which is much larger than that obtained with QCR.

Nomenclature

α	=	angle-of-attack
c_{ref}	=	mean aerodynamic chord
Ma	=	Mach number
Re_c	=	Reynolds number based on c_{ref}
T_∞	=	free stream temperature
cnts	=	drag coefficient unit=0.0001
η	=	fraction of wing span
C_L	=	lift coefficient
C_D	=	drag coefficient
C_{Dp}	=	pressure drag coefficient
C_{Dv}	=	viscous drag coefficient
C_m	=	pitching moment coefficient

[1] Ph.D. Candidate, College of Aerospace Engineering
[2] Assistant researcher, Computational Aerodynamics Institute
[3] Researcher, Computational Aerodynamics Institute
[4] Associate researcher, Computational Aerodynamics Institute
[5] Researcher, Computational Aerodynamics Institute

cp = pressure coefficient
C_{fx} = axial component of skin friction coefficient

I. Introduction

Reynolds-averaged Navier-Stokes (RANS) based Computational Fluid Dynamics (CFD) is now playing a more and more important role in the design process of aircraft industries. Subsequently CFD verification and validation have drawn extensive attentions among CFD researchers and vendors. To assess the state-of-the-art computational methods as practical aerodynamic tools for aircraft force and moment prediction of industry relevant geometries, the Applied Aerodynamics Technical Committee of the American Institute of Aeronautics and Astronautics (AIAA) initiated AIAA CFD Drag Prediction Workshop (DPW) Series in 2001. The workshop series provide an impartial forum to assess the numerical prediction capability (meshing, numerics, turbulence modeling, etc) for wing-body configurations and identify areas needing additional research and development. The latest workshop, DPW5, took place in June 2012. [1]

On inspection of the turbulence models adopted in DPW series, Spalart-Allmaras (SA) model and Menter Shear Stress Transport (SST) model are two of the most popular turbulence models in aircraft industries. The researchers have made various modifications to the original proposed models to account for the different problems emerging in implementations and applications. Most of the modifications generally retain the basic formulations of the models with only adding or modifying particular terms or minor modification of model constants. Mariani[2, 3] proposed the correction to SA model to reduce eddy viscosity in regions where vorticity exceeds strain rate, such as in vortex core regions where pure rotation should not produce turbulence. The reduction is achieved by lowering the production of the SA model in vortex dominated regions. The modification should recover to the original forms in thin shear layers where vorticity and strain are very close. The modification, hereinafter noted by Rotation Correction (RC), is proved to be superior to the original model in wing-tip vortex predictions. The Rotation Correction to the SST model was proposed by Hellsten[4] and Mani[5], where the destruction term in theωequation was multiplied by an artificial function to reduce the eddy viscosity in vortex dominated regions. Spalart[6, 7] performed the prediction of secondary vertical flows induced by Reynolds stress gradients acting in the corner regions in internal flows. The widely-used Boussinesq eddy-viscosity approximation was found to be inadequate for the prediction for lack of terms accounting for the anisotropy of the Reynolds-stress tensor. Spalart proposed a simple Quadratic Constitutive Relation (QCR) to introduce the anisotropy of the Reynolds-stress. The approach was shown to be simple to implement and overall agreement was seen to improve in predicting turbulence driven secondary flows in a square duct. Two versions, that are QCR2000 and QCR2013, are found in the literatures.

It is still an important issue as to which turbulence model or correction is superior in industries applications and far from being settled. To assess the effects of turbulence model corrections on drag prediction of NASA Common Research Model (CRM), which is the benchmark model of DPW 4&5, elaborate numerical simulations are performed. SA and SST model together with RC and QCR are taken into account. The detailed performances of the models and corrections are presented in this paper and comparisons are made between numerical results and experiment results.

II. Numerical methods

The computations are accomplished with in-house unstructured grids solver MFlow, which is based on cell-center finite volume method and capable of handling arbitrary element type. 2nd order accuracy in space is achieved with linear reconstruction in cells. The vertex-based Gauss method is adopted for gradient computations to fulfill accuracy and robustness simultaneously. Roe scheme is used for inviscid flux computations.

Fully turbulent is assumed in the computations. For SA model, the original form, RC, QCR2000 and QCR2013 are taken into account. For SST model, the original form, QCR2000 and QCR2013 are taken into account.

The original SA transport equation is given by the following:

$$\frac{\partial \tilde{\nu}}{\partial t}+u_j\frac{\partial \tilde{\nu}}{\partial x_j}=c_{b1}\left(1-f_{t2}\right)\tilde{S}\tilde{\nu}+\frac{1}{\sigma}\left[\frac{\partial}{\partial x_j}\left(\left(\nu+\tilde{\nu}\right)\frac{\partial \tilde{\nu}}{\partial x_j}\right)+c_{b2}\frac{\partial \tilde{\nu}}{\partial x_j}\frac{\partial \tilde{\nu}}{\partial x_j}\right]-\left[c_{w1}f_w-\frac{c_{b2}}{\kappa^2}f_{t2}\right][\frac{\tilde{\nu}}{d}]^2$$

where $\tilde{S}$ in the production term is defined as $\tilde{S}=\Omega+\frac{\tilde{\nu}}{\kappa^2 d^2}f_{v2}$.

In RC, the magnitude of vorticity Ω (in the $\tilde{S}$ production term) is replaced by:

$$\Omega + C_{rot}\min\left(0, S-\Omega\right)$$

The constant C_{rot} represents an attempt to empirically adjust the production term for vortex dominated flows. The value of 2 was recommended in Ref 3.

In QCR, the turbulent stress is defined as:

$$\tau_{ij,QCR} = \tau_{ij} - C_{r1}\left[O_{ik}\tau_{jk} + O_{jk}\tau_{ik}\right] - C_{r2}\mu_t\sqrt{2S^*_{mn}S^*_{mn}}\delta_{ij}$$

where τ_{ij} are the turbulent stresses computed from the Boussinesq relation, O_{ik} is an antisymmetric normalized rotation tensor. The constant is C_{r1}=0.3. In QCR2000, C_{r2}=0. In QCR2013, C_{r2}=2.5.

III. Geometry and Computational Grids

NASA CRM, the benchmark model of DPW 4&5, is composed of transonic supercritical wing and fuselage which is representative of a wide body commercial transport aircraft. The geometry details are provided in Ref. 8. Experiments were conducted in NASA Langley National Transonic Facility (NTF) and NASA Ames 11-ft[9]. The experiment results are presented in Figure 1. Detailed aerodynamic data has been generated and provided for CFD validation.

Corrections applied to experiment results must be kept in mind during CFD comparisons with experiment data. Wing aeroelastic twist is a remarkable factor according to the lessons learned from the DPW series. For medium to large aspect ratio wings, the local angle-of-attack shows evident difference with the free stream flow angle due to aerodynamic loading. Pseudo Test Data in Figure 1 is created from the NTF data and CFD analyses to reflect what the test data might look like for the wing without the "C_L=0.50 aeroelastic" twist10. There exists an evident shift in the curve of lift coefficient C_L and pitching moment coefficient Cm.

Two families of unstructured grids provided by the DPW committee are used in the computations. One family consists of only hexahedral elements while the other consists of prisms and tetrahedral elements. The grids information is given in Table 1. The series of hexahedral grids is labeled with L1T, L2C, L3M, L4F, L5X, where L1T stands for the coarsest grid while L5X for the finest grid. The number of grid cells ranges from 638976 to 40894464. The hybrid grid series is obtained by splitting a hexahedral element into two prisms near solid walls and into six tetrahedral elements elsewhere. The surface and symmetric plane grid is shown in Figures 2 and 3.

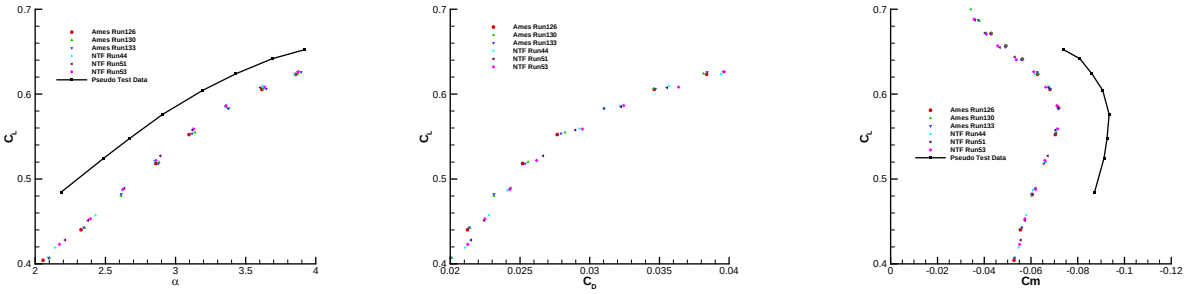

Figure 1. Experiment results of NASA CRM

Table 1. Information about the grids of CRM

Grid label		L1T	L2C	L3M	L4F	L5X
Hexahedral family		638976	2156544	5111808	17252352	40894464
Hybrid family	Total	2981888	10063872	24068096	80990208	/
	prism	425984	1437696	3301376	11261952	/
	tetra	2555904	8626176	20766720	69728256	/

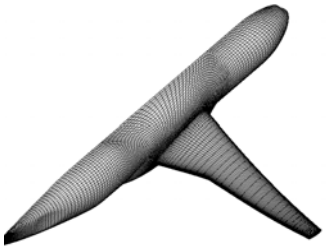

Figure 2. Surface grid（L1T of hexahedral series）

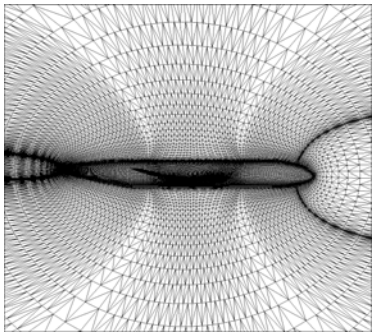

Figure 3. Symmetric plane grid（L2C of hybrid series）

IV. Results and discussions

The freestream conditions are Rec=5.0×106, Ma=0.85, T_∞=310.9K. The angles-of-attack in the computation range from 2^o to 4^o.

A. Grid convergence study with original SA model

Grid convergence study is an important process in verifying that numerical solutions are valid representations of the governing equations under investigation[11]. It can be used to identify the actual accuracy order of the solver and estimate the grid independent solution, which is the numerical solution when the number of grid cells approaches infinity.

The force and pitching moment prediction with the original SA model under a lift condition of C_L=0.5 is presented in Table 2. Numerical results with the two grid families and experiment data obtained in NTF are shown for comparison. It is evident that the prediction of angle-of-attack at which the desired lift coefficient is achieved shows a remarkable difference with reference experiment data. The similar trend was found in the former DPW series. According to the analysis of Neal T. Frink[12], many potential factors may account for the difference, including the model support system, wall interfere, model aeroelastic effects, transition and so on. Therefore, it is more meaningful to focus on the drag coefficient prediction under the same lift condition. The difference between drag predicted with two of the finest hexahedral grids (labeled with L4F and L5X) and reference experiment is within 2 cnts. Therefore the drag prediction under the cruise lift condition is satisfied. Pressure drag is more sensitive to grid refinement than viscous drag. For the hexahedral series, the pressure drag decreases 17.4 cnts form the coarsest grid to the finest grid, while the viscous drag increases 4.4 cnts. This may suggest that even the coarsest grid in the series is sufficient for the prediction of boundary velocity profile. Even the coarsest grid has reasonably fine wall-normal spacing, giving an approximate average y+=0.72. The trend is more evident for the hybrid series. The pressure drag decreases 23.1 cnts form the coarsest grid to the finest grid, while the viscous drag increases only 2.9 cnts.

The effects of element types in drag prediction can also be found in Table 2. Drag predicted with hexahedral grid is smaller than that with hybrid grid with the same label. The difference is mainly due to pressure drag prediction. The viscous drag and pitching moment show minor difference. The conclusion that hexahedral grid is superior than hybrid grid in drag prediction can't be made before hybrid grid is redesigned and hence not obtained by splitting hexahedral grids.

Table 2 numerical results with original SA model

Grid type	Hexahedral elements					Hybrid elements				NTF
Grid label	L1T	L2C	L3M	L4F	L5X	L1T	L2C	L3M	L4F	/
A(^{o})	2.263	2.210	2.194	2.174	2.165	2.298	2.228	2.199	2.181	2.791
CD(cnts)	263.0	254.6	252.0	250.8	250.1	277.4	266.0	261.4	257.3	248.9
CDp(cnts)	152.3	141.4	138.0	135.8	134.9	165.6	152.3	147.2	142.5	/
CDv(cnts)	110.7	113.3	113.9	114.9	115.1	111.8	113.7	114.2	114.7	/
Cm	-0.1079	-0.1124	-0.1136	-0.1152	-0.1157	-0.1078	-0.1124	-0.1144	-0.1152	-0.06313

The grid convergence behaviors of results obtained with the hexahedral grid series are shown in Figure 4. The horizontal coordinate stands for $N^{-2/3}$, where N is the total cell number. The solver is designed to achieve 2nd order accuracy in space, therefore $N^{-2/3}$ stands for the square of typical cell scale for a series of nested grids. If the solver is correctly established and the grid series is located among the asymptotic range of convergence, the force and moment should display linear behavior in the grid convergence curves. It is shown in Fig. 4 that the drag, pitching moment and angle-of-attack all achieve nearly linear grid convergence with grid refinement, which implies that the actual accuracy order of the solver is 2nd and the solutions are in the asymptotic range. The solutions obtained with the hybrid grid series also show nearly linear convergence with grid refinement (not shown in this paper). Through the linear grid convergence curves, the grid independent solution can be estimated.

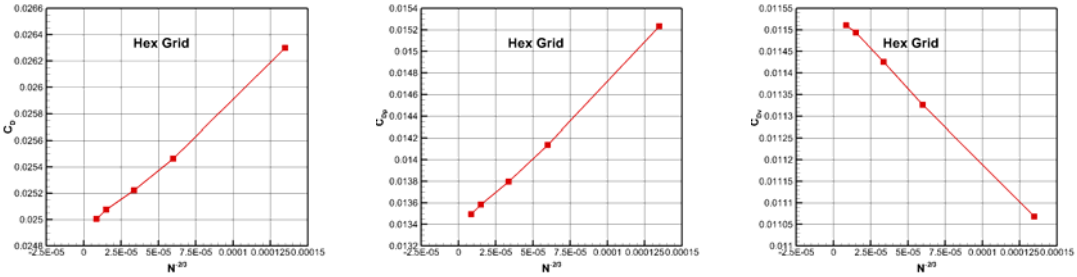

(a) total drag **(b) pressure drag** **(c) viscous drag**

Figure 4. Grid convergence of drag (hexahedral series)

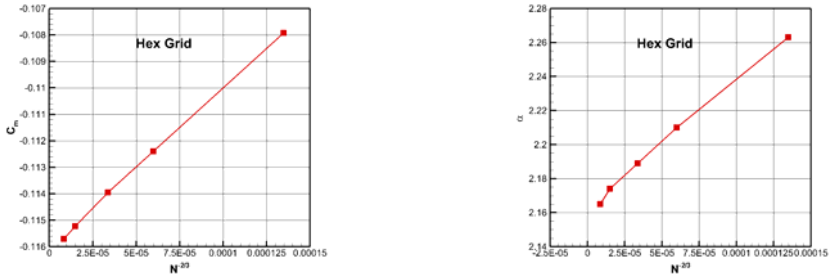

(a) angles-of-attack **(b) pitching moment**

Figure 5. Grid convergence of angles-of-attack and pitching moment (hexahedral series)

The comparison of pressure distribution prediction with the hexahedral grid series under the lift condition of C_L=0.5 is presented in Figure 6. Three span wise slices are considered, that is 0.1050, 0.3700 and 0.9500, which are representative of cuts from wing root to wing tip. The effect of grid refinement only shows itself in the resolution of shock wave and the difference is minor elsewhere. The locations of shock wave obtained with two of the finest grids are almost identical, which also proves the grid convergence of surface pressure prediction. The result obtained with the coarsest grid shows remarkable difference with that obtained with finer grids, leading to the over predicted pressure drag.

The surface streamlines near the wing-body junction with hybrid element series are presented in Figure 7. The blue regions denote regions with negative C_{fx}, which can be used to identify separation near solid walls. Separation bubble at wing-body junction is more clearly resolved with grid refinement and the size of the bubble is larger. The author ever conducted simulations with the more dissipative Steger Warming scheme for comparison. Under the same conditions, the dissipation of numerical schemes also influences the resolution of this side-of-body bubble. The size of the bubble is much decreased with Steger Warming scheme.

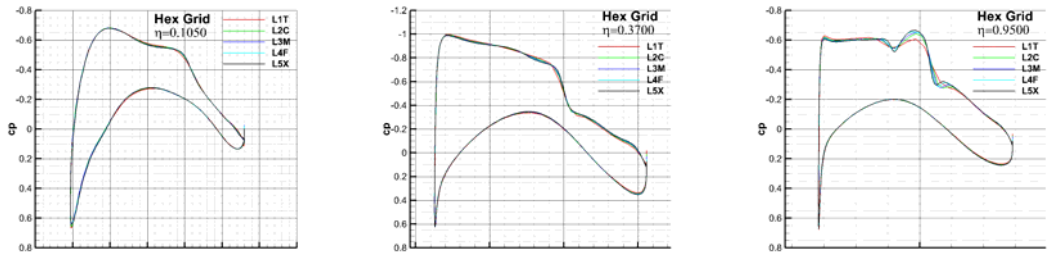

(a) η=0.1050 **(b) η=0.3700** **(c) η=0.9500**

Figure 6. Comparison of pressure distribution prediction (hexahedral series)

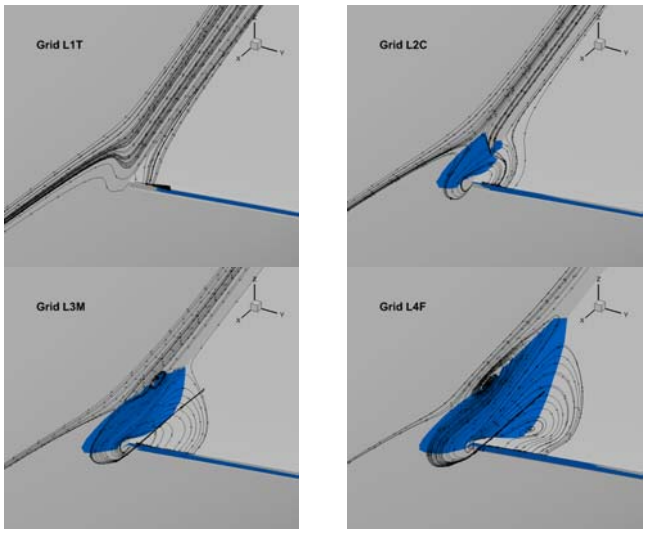

Figure 7. Comparison of surface streamlines (hybrid series)

B. The effects of turbulence model corrections

The effects of turbulence models and corrections on force and moment prediction under the lift condition of C_L=0.5 are presented in Table 3. The medium hexahedral grid with the label L3M is used. For SA model, the difference of viscous drag among different formulations is much smaller than that of pressure drag. The largest difference in viscous drag prediction is between original form and QCR2013, with 0.9 cnts. The largest difference in pressure drag is 3.2 cnts. RC and QCR slightly decrease the viscous drag while increase pressure drag dramatically, leading to the increase of total drag. The same trends are found with SST model.

Table 3. Comparison of results with different model corrections under the lift condition of C_L=0.5

Model corrections	C_D(cnts)	C_{Dp}(cnts)	C_{Dv}(cnts)	C_m	A(^{o})
SA	252.0	138.0	113.9	-0.11363	2.194
SA_RC	252.0	138.7	113.3	-0.11235	2.205
SA_QCR2000	253.7	140.3	113.4	-0.10960	2.235
SA_QCR2013	254.2	141.2	113.0	-0.10852	2.251
SST	252.5	141.8	110.7	-0.10540	2.290
SST_QCR2000	254.5	144.5	110.0	-0.10103	2.336
SST_QCR2013	255.2	145.5	109.7	-0.09981	2.354

The force and moment curves are presented in Figure 8. The NTF data and pseudo test data are only shown for reference. More attention is paid to obtain the effects of model corrections on aerodynamic characteristics prediction,

not to compare numerical results to this "plausible" experiment data. At small to medium angles-of-attack, the difference between original forms and corrections is minor. The scatter is significantly larger at medium to large angles. All the curves show similar trends, which implies that under the same conditions, the corrections do not make qualitative changes to the flow patterns and may only influence the flow field details such as separation or shock wave location. For SA model, at AoA=4°, the lift coefficient obtained with original forms are largest followed by RC, QCR2000 and QCR2013. The contours of pressure coefficient obtained with model corrections minus that with original forms are presented in Figure 9. It is evident that model corrections mainly influence the pressure prediction near the shock wave. Relative to the original form, the model corrections, especially QCR, achieve larger pressure coefficient near shock wave which extends from wing tip to wing root. The pressure distribution along the η=0.5024 slice in Figure 10 clearly shows the location of shock wave is shifted upstream due to model corrections. RC has the effect of reducing the eddy viscosity, which results in the capability of the boundary layer to persist under adverse pressure gradients weakening. The effect is more evident with QCR.

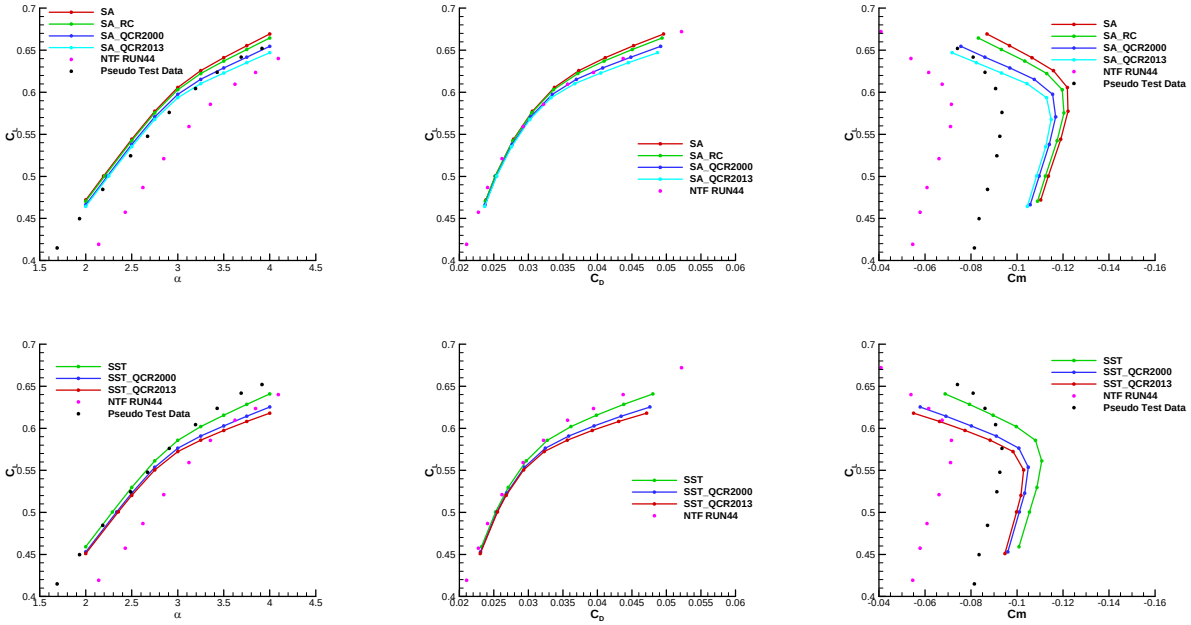

Figure 8. Comparison of force and moment curve

Figure 9. Contours of surface pressure distribution with different model corrections (AoA=4°)

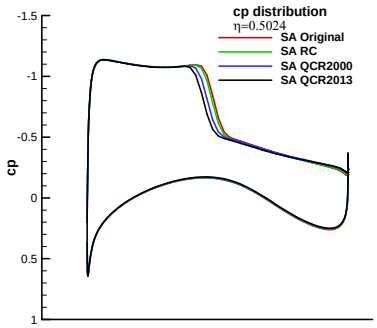

Figure 10. Comparison of pressure distribution along mid span cut (AoA=4°)

Besides the location of shock wave on the wing upper surface, model corrections also influence the prediction of side-of-body bubbles. The contours of C_{fx} and surface streamlines near wing-body junction are presented in Figure 11. The size of the bubble is very close between results obtained with the original form and RC, which is much larger than that obtained with QCR. Here only the trend is given, not the judgement, because of the uncertain flow pattern in reality.

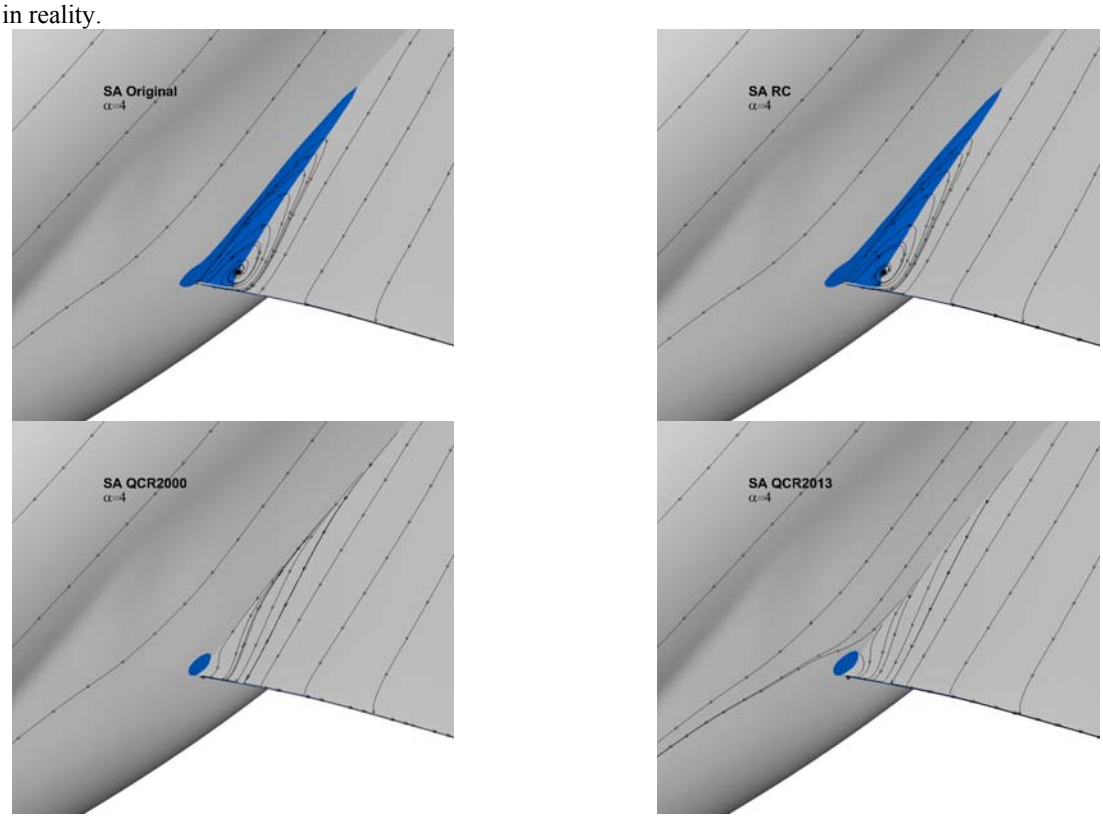

Figure 11. Comparison of surface streamlines with different model corrections

V. Conclusion

The effects of the turbulence model corrections on drag prediction of the NSAS CRM are investigated in this paper with in-house solver MFlow. Two series of unstructured grids supplied by the DPW committee are used in computations. For the original SA model, under the lift condition of C_L=0.5, nearly linear grid convergence is achieved for drag and moment prediction. The difference between drag predicted with the two finest hexahedral grids and reference experiment is within 2 cnts, which is satisfied.

All the aerodynamic curves with different corrections show similar trends. Model corrections mainly influence the pressure prediction near the shock wave. Relative to the original form, the model corrections, especially QCR, achieve larger pressure coefficient near shock wave which extends from wing tip to wing root. The location of shock wave is shifted upstream due to model corrections. Model corrections also influence the prediction of side-of-body bubbles. The size of the bubble is very close between results obtained with the original form and RC, which is much larger than that obtained with QCR.

Only the trends brought by the model corrections are presented in this paper. Which turbulence model or correction is superior in industries is far from being settled.

References

[1]http://aaac.larc.nasa.gov/tsab/cfdlarc/aiaa-dpw.

[2]Dacles-Mariani J., Zilliac G. G., Chow J. S., and Bradshaw P. Numerical/Experimental Study of a Wingtip Vortex in the Near Field. AIAA Journal, Vol. 33, No. 9, 1995, pp. 1561-1568.

[3]Dacles-Mariani J., Kwak D., and Zilliac G. G. On Numerical Errors and Turbulence Modeling in Tip Vortex Flow Prediction, Int. J. for Numerical Methods in Fluids, Vol. 30, 1999, pp. 65-82.

[4]Hellsten, A., Some Improvements in Menter's k-omega SST Turbulence Model, AIAA-98-2554, June 1998.

[5]Mani, M., Ladd, J. A., and Bower, W. W., Rotation and Curvature Correction Assessment for One- and Two-Equation Turbulence Models, Journal of Aircraft, Vol. 41, No. 2, 2004, pp. 268-273.

[6]Spalart, P. R., Strategies for Turbulence Modelling and Simulation, International Journal of Heat and Fluid Flow, Vol. 21, 2000, pp. 252-263.

[7]Mani, M., Babcock, D. A., Winkler, C. M., and Spalart, P. R., Predictions of a Supersonic Turbulent Flow in a Square Duct, AIAA Paper 2013-0860, January 2013.

[8]John C V, Mark A D. Development of a Common Rese-arch Model for Applied CFD Validation Studies. AIAA-2008-6919.

[9]Melissa B R, Ashley D. Experimental Investigation of the NASA Common Research Model in the NASA Langley National Transonic Facility and NASA Ames 11-ft Transonic Wind Tunnel. AIAA-2011-1126.

[10]David W. Levy, Kelly R. Laflin, Edward N. Tinoco, John C. Vassberg, Mori Mani, Ben Rider, Chris Rumsey, RicharA. Wahls, Joseph H. Morrison, Olaf P. Brodersen, Simone Crippa, Dimitri J. Mavriplis and Mitsuhiro Murayama. Summary of Data from the Fifth AIAA CFD Drag Prediction Workshop. AIAA-2013-0046.

[11]Salas, M. D., "Some Observations on Grid Convergence," Computers & Fluids, Vol. 35, No. 7, 2006, pp. 688-692.

[12]Shahyar Z. Pirzadeh, Neal T. Frink. Assessment of the U-nstructured Grid Software TetrUSS for Drag Prediction of the DLR-F4 Configuration. AIAA-2002-083.